International Journal of Thermophysics, Vol. 25, No. 4, July 2004 (© 2004)

Thermophysical Properties of Binary Mixtures of R125 + R143a in Comparison with a Simple Prediction Method[1]

A. P. Fröba,[2] H. Kremer,[2] and A. Leipertz[2,3]

The thermal diffusivity and sound speed of binary refrigerant mixtures of R143a (1,1,1-trifluoroethane) and R125 (pentafluoroethane) have been determined for both the saturated liquid and vapor phase using dynamic light scattering (DLS). Measurements were performed for four quite different mixture compositions over a wide temperature range from 293 to 345 K approaching the vapor-liquid critical point. The results obtained corroborate the usefulness of a simple prediction method for the determination of different thermophysical properties of multicomponent mixtures in the two-phase region up to the critical point. Besides the information on the properties for the pure components, the successful application of the prediction method is also based on an exact knowledge of the critical temperature. The composition dependence of the critical temperature has been determined by observation of the vanishing meniscus between liquid and vapor phases. The mixture results are discussed in detail and compared with available literature data.

KEY WORDS: binary mixture; dynamic light scattering; 1,1,1-trifluoroethane, pentafluoroethane; sound speed; thermal diffusivity.

1. INTRODUCTION

In technical applications working fluids are mostly mixtures of several pure components, as the properties of these mixtures are adjustable to

[1]Paper presented at the Fifteenth Symposium on Thermophysical Properties, June 22–27, 2003, Boulder, Colorado, U.S.A.

[2]Lehrstuhl für Technische Thermodynamik (LTT), Friedrich-Alexander-Universität Erlangen-Nürnberg, Am Weichselgarten 8, D-91058 Erlangen, Germany

[3]To whom correspondence should be addressed. E-mail: sek@ltt.uni-erlangen.de

0195-928X/04/0700-1115/0

a certain extent by their composition to meet the various technical requirements. For the design of technical processes using these mixtures, their thermophysical properties have to be known. Taking, however, the huge number of possible mixtures into consideration, it is obvious that the ensemble of thermophysical properties of every conceivable mixture cannot be obtained by carrying out appropriate measurements. Alternatively, prediction methods for the mixture properties are necessary [1]. Regrettably, these prediction methods differ in their complexity, applicability, and accuracy. Particularly for the daily practice in technical applications it is of high importance to find the thermophysical properties of working fluids with sufficient accuracy in a quite simple way. However, most prediction methods which are easy to use, e.g., simple mixing rules, exhibit a lack of accuracy and are, in most cases, only applicable within a narrow region of conditions [2].

Using dynamic light scattering (DLS) we have reported the thermal diffusivity and sound speed of the refrigerant mixtures R507 (50 mass % R125, 50 mass % R143a) and R404A (44 mass % R125, 52 mass % R143a, 4 mass % R134a) under saturation conditions for both the liquid and vapor phases over a wide temperature range approaching the liquid–vapor critical point [3]. Beside testing the applicability of the DLS-technique to multicomponent mixtures and improving the data situation for refrigerant mixtures of technical importance, the interest of our previous work was directed to a comparison of the experimental results with simple prediction methods. These results have suggested that the mixture data for both thermal diffusivity and sound speed can best be represented by the mass weighted sum of the pure component data expressed as functions of the reduced temperature. The properties of the mixture Y_M under saturation conditions have thus been predicted according to

$$Y_M(T_R) = \sum_j w_j Y_j(T_R), \tag{1}$$

where w_j and Y_j are the mass fraction and the property at the reduced temperature $T_R = T/T_C$ of component j, respectively, and T is the absolute temperature and T_C is the critical temperature.

The motivation for further experimental investigation of the binary refrigerant system of R125 and R143a was established by the question whether this simple approach, successfully applied for the mixtures R507 and R404A, can also be used for any other mixture composition of these pure components. Thus, in the present work we focused our

investigation on four binary mixtures of R125 and R143a with quite different compositions. In the following, at first the methodological principles of DLS for the determination of thermal diffusivity and sound speed are briefly reviewed. For a more detailed and comprehensive description of the underlying theory of DLS from bulk fluids, the reader is referred to the specialized literature [4–6]. Then, the experimental results for the four binary mixtures of R125 and R143a with quite different compositions are presented and compared with the proposed prediction method based on the properties of the pure components expressed as functions of the reduced temperature.

2. EXPERIMENTAL METHOD

When a fluid sample in macroscopic thermodynamic equilibrium is irradiated by coherent laser light, light scattered from the sample can be observed in all directions. The underlying scattering process is governed by microscopic fluctuations of temperature (or entropy), of pressure, and of species concentration in mixtures. The relaxations of these statistical fluctuations follow the same rules that are valid for the relaxation of macroscopic systems. Thus, the decay of temperature fluctuations is governed by the thermal diffusivity a. Pressure fluctuations in fluids are moving with a sound speed u_S and their decay is governed by the sound attenuation D_S. In a binary fluid mixture the decay of concentration fluctuations is governed by the mutual diffusion coefficient D_{12}.

In light scattering experiments the above-mentioned equalization processes result in a temporal modulation of the scattered light intensity. Information about these processes can be derived through a temporal analysis of the scattered light intensity using photon correlation spectroscopy (PCS). For heterodyne conditions, where the scattered light is superimposed with stronger coherent reference light, the time-dependent intensity correlation function for the analysis of the temperature fluctuations is described by

$$G^{(2)}(\tau) = A + B \exp(-\tau/\tau_C), \tag{2}$$

where A and B are experimental constants, which are essentially determined by total number of counts registered, the ratio of scattered light to reference light, and the coherence properties of the optical system. From the correlation time τ_C, which is equivalent to the mean lifetime of the temperature fluctuations observed, the thermal diffusivity a can be calculated by

$$a = \frac{1}{\tau_C q^2}, \tag{3}$$

where the modulus of the scattering vector q is determined beside the laser wavelength in vacuo by the scattering geometry of the experiment, see, e.g., Ref. 6.

For the measurement of sound speed u_S the pressure fluctuations are probed. In practice, the frequency ω_S of the sound waves is determined by adding a reference beam, which is shifted relative to the frequency ω_0 of the laser light by $\Delta\omega_M$ applying an acousto-optical modulator. The frequency shift $\Delta\omega_M$ is of the same order of magnitude as the frequency of the sound waves ($\Delta\omega_M \approx \omega_S$). In this case, the correlation function takes the form,

$$G^{(2)}(\tau) = A + B \exp(-\tau/\tau_C)\cos(\Delta\omega\tau), \tag{4}$$

and the sound speed u_S can be found from a knowledge of the adjusted modulator frequency $\Delta\omega_M$ and the residual detuning $\Delta\omega$ according to

$$u_S = \frac{\omega_S}{q} = \frac{\Delta\omega_M \pm \Delta\omega}{q}. \tag{5}$$

Whether it is possible to determine signals from concentration fluctuations is mainly governed by the relative difference of the refraction indices of the mixture components and their concentration. For the refrigerant mixtures studied in this work the refractive indices of the pure components have comparable values [7,8]. Thus, only the scattered light signals from temperature and pressure fluctuations can be resolved which are associated with the thermal diffusivity and the sound speed, respectively.

3. EXPERIMENTAL

The experimental setup used here is essentially the same as was employed in former investigations and is described in more detail elsewhere, see, e.g., Refs. 9 and 10. Light from an argon ion laser ($\lambda_0 = 488\,\text{nm}$) operating in a single longitudinal mode was irradiated through a quartz window of the sample cell. The laser power was up to 160 mW when working far away from the critical point, and only a few mW in the critical region. The angle of incidence, which is defined as the angle between the optical axes of incidence and detection and from which the modulus of the scattering vector q can be deduced, was measured by

back-reflection from a mirror, mounted to a precision rotation table. For the experiment the angle of incidence was set between 3.5° and 6.0°. The error in the angle measurement has been determined to be approximately ±0.014° which results in a maximum uncertainty of less than 1% for the desired thermophysical properties. The detection optics simply consist of two circular stops with diameters of 1 and 2 mm. For large scattering intensities, scattered reference light from the cell windows alone was not sufficient to realize heterodyne conditions. Here, an additional reference beam originated by a beam splitter was superimposed to the scattered light. For the determination of sound speed, a reference beam shifted in frequency by an opto-acoustic modulator was added to the scattered light. The time-dependent intensity of the scattered light was detected by two photomultiplier tubes (PMTs) operated in cross-correlation in order to suppress after-pulsing effects. The signals were amplified, discriminated, and fed to a stand-alone correlator with 112 linearly spaced channels being operated with a sample time of 100 ns for the sound speed measurements and with a sample time between 0.5 and 20 μs chosen in such a way that the correlation function covers about six decay times for the thermal diffusivity measurements.

The refrigerant samples were filled into an evacuated cylindrical pressure vessel (volume $\approx 10\,\mathrm{cm}^3$) from the liquid phase to avoid fractionation, because the mixtures represent near-azeotropic mixtures. According to the specification of the manufacturer (Solvay Fluor and Derivate GmbH, Hannover), the refrigerant mixtures had a purity of $\geqslant$99.5 %. They were used without further purification. The composition (on a mass basis) for the investigated mixtures is given in Table I, where the results of the weighed sample are listed. For each mixture the uncertainty in the composition can be assumed to be ± 0.2 % which was confirmed by a gas-chromatographic analysis.

The actual temperature in the sample cell, which was placed in a multi-stage thermostat with a long-term stability better than 2 mK, was regulated through resistance heating. The temperature of the sample was measured with three calibrated 25 Ω platinum resistance probes integrated into the main body of the measuring cell with a resolution of 0.1 mK using an ac bridge (Paar, MKT 25). The uncertainty of the absolute temperature measurement was estimated to be less than ±15 mK. For each temperature point, typically six measurements at different angles of incidence were performed where the laser was irradiated from either side with respect to the axis of observation in order to check for a possible misalignment. The measurement times for a single run were typically of the order of ten minutes, decreasing to one minute for the highest temperatures in this study.

Table I. Experimental Values of the Thermal Diffusivity a and Sound Speed u_S of Binary Mixtures of R143a and R125 under Saturation Conditions

Thermal diffusivity				Sound speed			
Liquid phase		Vapor phase		Liquid phase		Vapor phase	
T (K)	a (10^{-8} $m^2 \cdot s^{-1}$)	T (K)	a (10^{-8} $m^2 \cdot s^{-1}$)	T (K)	u_S ($m \cdot s^{-1}$)	T (K)	u_S ($m \cdot s^{-1}$)
19.35 mass % R143a/80.65 mass % R125							
293.16	3.68	315.15	9.25	293.15	372.3	315.15	114.7
303.12	3.42	317.14	8.55	303.12	322.3	317.14	113.1
313.08	3.06	319.14	7.87	313.08	269.9	319.14	111.4
323.13	2.69	321.14	7.23	323.13	213.7	321.14	109.7
328.13	2.38	323.14	6.51	328.13	183.7	323.14	108.0
333.12	1.94	325.14	5.85	333.12	150.2	325.14	106.1
335.12	1.69	327.14	5.19	335.11	135.8	327.14	104.2
337.11	1.37	329.13	4.51	337.11	120.5	329.13	102.2
338.11	1.18	331.13	3.90	338.11	112.0	331.13	100.0
339.11	0.932	333.12	3.27	339.11	103.0	333.12	97.61
340.11	0.641	335.11	2.57	340.11	93.24	335.11	95.17
340.61	0.458	337.11	1.84	340.61	88.14	337.11	92.39
341.10	0.272	339.11	1.10	341.10	82.82	339.11	89.11
		340.11	0.720			340.10	86.84
		340.60	0.529			340.60	85.10
		341.10	0.331			341.10	82.87
39.88 mass % R143a/60.12 mass % R125							
293.39	3.86	315.14	9.97	293.23	386.9	315.13	119.7
303.16	3.56	319.13	8.57	303.16	337.0	319.13	117.0
313.16	3.25	323.13	7.30	313.16	284.3	323.13	113.6
323.15	2.86	327.12	5.86	323.15	228.5	327.12	110.1
328.14	2.60	331.12	4.51	328.15	198.2	331.12	105.9
333.14	2.16	335.12	3.14	333.14	165.8	335.12	101.3
337.13	1.68	339.11	1.76	337.13	136.8	339.11	95.70
339.13	1.33	341.11	0.973	339.12	120.8	341.11	92.24
340.12	1.10	342.11	0.595	340.12	112.1	342.11	89.12
341.12	0.838	342.91	0.284	341.12	102.9	342.91	86.79
342.11	0.510			342.12	93.17		
342.91	0.196			342.91	81.57		
59.00 mass % R143a/41.00 mass % R125							
293.31	4.05	318.14	9.51	293.25	398.6	318.14	122.4
303.15	3.76	320.14	8.83	303.15	348.6	320.14	120.8
313.14	3.46	324.14	7.40	313.14	295.7	324.14	117.5
323.13	3.03	328.13	5.95	323.13	239.8	328.13	113.8
328.13	2.73	332.13	4.61	328.13	209.4	332.12	109.5
333.12	2.37	336.12	3.23	333.12	177.1	336.12	104.9
338.11	1.75	340.11	1.77	338.11	141.0	340.11	99.37
340.11	1.39	342.11	1.01	340.11	124.7	342.11	95.43

Table I. *(Continued)*

Thermal diffusivity				Sound speed			
Liquid phase		Vapor phase		Liquid phase		Vapor phase	
T (K)	a (10^{-8} $m^2 \cdot s^{-1}$)	T (K)	a (10^{-8} $m^2 \cdot s^{-1}$)	T (K)	u_S ($m \cdot s^{-1}$)	T (K)	u_S ($m \cdot s^{-1}$)
342.10	0.884	343.10	0.614	342.10	106.3	343.10	92.94
343.10	0.547	343.61	0.420	343.10	96.17	343.60	90.49
343.60	0.346	344.00	0.264	343.60	90.95	344.00	88.29
344.00	0.177			344.00	86.16		
79.13 mass % R143a/20.87 mass % R125							
293.15	4.24	319.14	9.73	293.15	411.9	319.14	127.3
303.15	3.97	321.14	8.83	303.15	362.0	321.14	125.6
313.15	3.61	323.14	8.13	313.15	308.3	323.14	123.9
323.13	3.20	325.13	7.48	323.13	251.6	325.13	122.1
328.02	2.93	327.13	6.75	328.01	222.2	327.13	120.2
333.12	2.55	329.13	6.05	333.12	189.5	329.13	118.2
338.12	1.99	331.13	5.34	338.12	153.4	331.13	116.2
340.11	1.67	333.12	4.68	340.12	137.7	333.12	113.9
342.11	1.22	335.12	4.00	342.11	120.0	335.12	111.5
343.11	0.926	337.12	3.28	343.12	110.4	337.12	109.1
344.11	0.584	339.12	2.58	344.11	100.1	339.12	106.3
344.61	0.380	341.11	1.82	344.61	94.50	341.11	103.1
345.11	0.133	343.10	1.04	345.11	90.58	343.10	98.60
		344.12	0.603			344.11	96.21
		344.62	0.377			344.62	94.34
		345.10	0.171			345.11	92.85

4. RESULTS AND DISCUSSION

4.1. Measurement Data for Thermal Diffusivity and Sound Speed

The experimental data for the thermal diffusivity and sound speed of binary mixtures of R125 and R143a obtained by light scattering from bulk fluids are summarized in Table I. In Fig. 1, in addition to the mixture data obtained in this work, the pure component data and the data for R507 (50 mass % R125/50 mass % R143a) are shown, the last obtained from our previous investigation [3, 11–13]. The lines are empirical correlations of the experimental data. For the mixtures each temperature point comprises six single measurements, the mean value of which is displayed. The standard deviation of the single measurements may be regarded as a measure of the uncertainty of DLS data [14]. For reduced temperatures $T_R < 0.99$ the uncertainties of the measured mixture data are estimated to

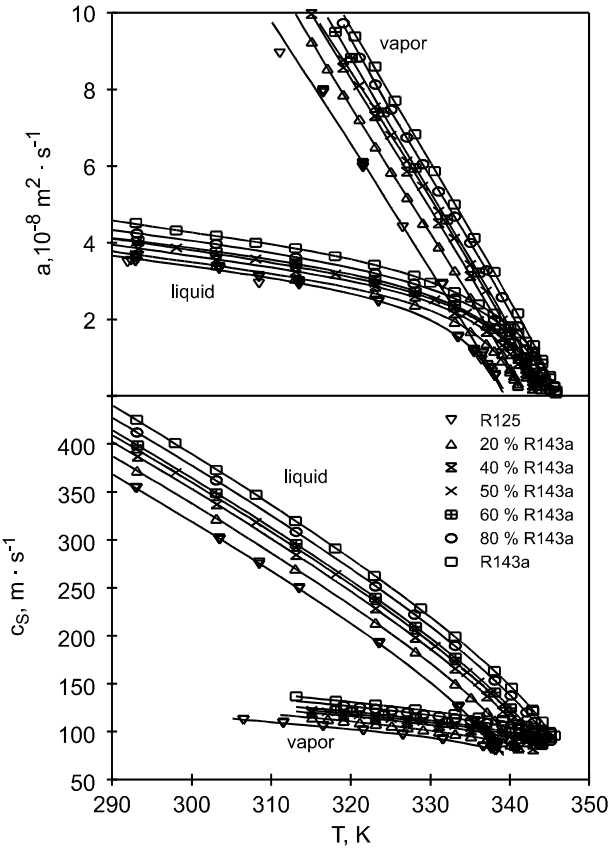

Fig. 1. Thermal diffusivity and sound speed of the binary mixture R-125/143a for five different compositions (in mass %) under saturation conditions as a function of temperature.

be less than ±1 % for the thermal diffusivity and less than ±0.5 % for the sound speed. For the highest temperatures ($T_R > 0.99$) studied in this work, the measurement uncertainty for the thermal diffusivity and sound speed increases to about ±2 % and ±1 %, respectively. The reason for this behavior can be found by an increasing experimental complexity in the critical region.

The overall uncertainty of our mixture data including the uncertainty in the composition is of course somewhat larger. This effect could be estimated with the help of the simple prediction method given by Eq. (1). For the thermal diffusivity the uncertainty in the composition may result in an additional uncertainty up to a maximum of ±0.4 % for both the saturated

vapor and liquid phases. An additional uncertainty of ±0.4 % and ±0.3 % introduced by the uncertainty in the composition could be estimated for the sound speed in the vapor and liquid phases, respectively.

4.2. Data Correlation

The experimental mixture data for the thermal diffusivity as well as for the sound speed for both vapor and liquid phases can be well represented by a sum of a polynomial and an additional term, which takes into account the curvature towards the critical point, resulting in an equation of the form,

$$y = \sum_{i=0}^{2} y_i (T/\mathrm{K})^i + \frac{y_3}{(T - T_C^*)/\mathrm{K}}, \tag{6}$$

where the coefficients y_i and the additional fit parameter T_C^* are given in Table II. Here, also the root-mean-square deviations of our values from Eq. (6) and the ranges of validity of the correlations are given. For both phases the root-mean-square deviations of our sound speed data from Eq. (6) are clearly less than 0.5 %. Somewhat worse is the situation for the thermal diffusivity data, where a maximum root-mean-square deviation of 1.12 % can be found for the saturated vapor phase of the mixture with 59 mass % R143a and 41 mass % R125. Equation (6) is quite similar to a general approach as proposed by Friend and Perkins [15] for fitting transport properties over a wide temperature range at saturation approaching the vapor–liquid critical point. Yet, they have suggested only four adjustable parameters using the true critical temperature T_C instead of T_C^*. However, since the saturation values in particular for the thermal diffusivity are vanishing as the critical point is approached, such a type of equation fails to reasonably represent our data for the whole temperature range. Thus, we have chosen the empirical approach Eq. (6) with an additional adjustable parameter T_C^* so that the critical behavior can be described more correctly, and moreover, by extrapolating Eq. (6), the values in particular for the thermal diffusivity are vanishing at $T = T_C$.

4.3. Visual Observation of the Vapor–Liquid Critical Point

Our first interest was directed to the comparison of the experimental mixture data with the simple prediction method according to Eq. (1) which is based on the properties of the pure component data expressed as functions of the reduced temperature. Thus, a successful application of the simple prediction method requires, in addition to the

Table II. Coefficients of Eq. (6)

	Thermal diffusivity a y_i ($10^{-8}\,m^2 \cdot s^{-1}$)		Sound speed u_S y_i ($m \cdot s^{-1}$)	
y_i	Liquid phase	Vapor phase	Liquid phase	Vapor phase
19.35 mass % R143a/80.65 mass % R125				
y_0	20.357	386.52	1182.64	−603.15
y_1	−0.09062	−2.0725	−0.7214	5.2913
y_2	0.12043×10^{-3}	2.79919×10^{-3}	-6.8586×10^{-3}	-9.559×10^{-3}
y_3	25.299	96.989	548.62	9.7
T_C^*(K)	349.043	360.686	350.946	342.565
T-range (K)	293–341	315–341	293–341	315–341
rms (%)	0.60	0.93	0.09	0.08
39.88 mass % R143a/60.12 mass % R125				
y_0	28.2874	131.608	717.06	−684.48
y_1	−0.1428427	−0.433038	2.5344	5.7618
y_2	0.209632×10^{-3}	0.150074×10^{-3}	-12.4332×10^{-3}	-10.1785×10^{-3}
y_3	33.234	2.708	247.61	21.0
T_C^* (K)	351.760	348.494	348.826	345.621
T-range (K)	293–343	315–343	293–343	315–343
rms (%)	0.76	1.20	0.49	0.16
59.00 mass % R143a/41.00 mass % R125				
y_0	9.41506	292.948	1223.9	−697.99
y_1	−0.0152803	−1.435419	−0.7848	5.9014
y_2	-5.2449×10^{-6}	1.721431×10^{-3}	-6.7932×10^{-3}	-10.4397×10^{-3}
y_3	25.612	41.246	673.69	11.6
T_C^* (K)	351.615	359.773	354.563	345.375
T-range (K)	293–344	318–344	293–344	318–344
rms (%)	0.60	1.12	0.08	0.10
79.13 mass % R143a/20.87 mass % R125				
y_0	8.80455	1040.6433	1143.02	9.84
y_1	−0.0081533	−6.3043216	−0.1602	1.5124
y_2	-20.4566×10^{-6}	10.013197×10^{-3}	-7.8162×10^{-3}	-3.5609×10^{-3}
y_3	24.214	3124.771	781.11	78.6
T_C^* (K)	352.195	399.5736	356.745	350.380
T-range (K)	293–345	319–345	293–345	319–345
rms (%)	0.61	0.56	0.38	0.09

information about the pure component data, an accurate knowledge of the mixture critical temperature. If this information is not available, significant errors may be introduced by the model especially in approaching the vapor-liquid critical point. For our previous investigations with R507 (50 mass % R125/50 mass % R143a) in the saturated liquid phase, the influence of the uncertainty in the critical temperature on the simple prediction method is shown in Fig. 2. In using Eq. (1) for predictions of

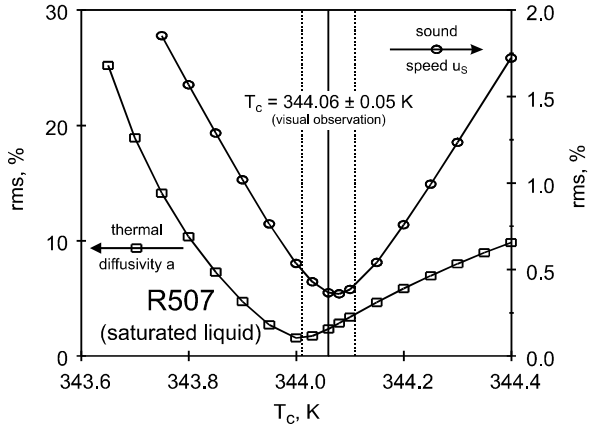

Fig. 2. Root-mean-square deviations of the measured data for the binary mixture R507 (50 mass % R125/50 mass % R143a) in the saturated liquid phase from the prediction method and their dependence on the mixture critical temperature.

thermal diffusivity and sound speed, the root-mean-square deviations of the experimental data from the predictions are kept to minimum values of about 1.6 % and 0.4 %, respectively, if the exact value for the critical temperature of 344.06 ± 0.05 K is applied. This value has been obtained by visual observation of the vanishing meniscus between the liquid and vapor phases when approaching the critical point [3]. However, a change in the critical temperature of only 0.5 K yields a remarkable increase of the root-mean-square deviation. In consequence, the uncertainty of the prediction method increases rapidly with an increasing error in the mixture critical temperature.

In the present work again the method of the vanishing meniscus between liquid and vapor phases has been applied for the determination of the mixture critical temperature. Regarding a successful application of the simple prediction method the observation of the vanishing meniscus allows the determination of the mixture critical temperature with reasonable certainty; (see Fig. 2). The results of our observations for the critical temperatures of binary mixtures of R125 and R143a are summarized in Table III and are plotted in Fig. 3 showing their dependence on the mass fraction w_{R143a} of R143a. In Table III the critical temperatures of the pure components R125 [16] and R143a [17] and of the binary mixture R507 [3] are also given. It is obvious that the composition dependence of the critical temperature of the binary mixture of R125 and R143a does not follow a mass-weighted sum of the critical temperatures of the pure components

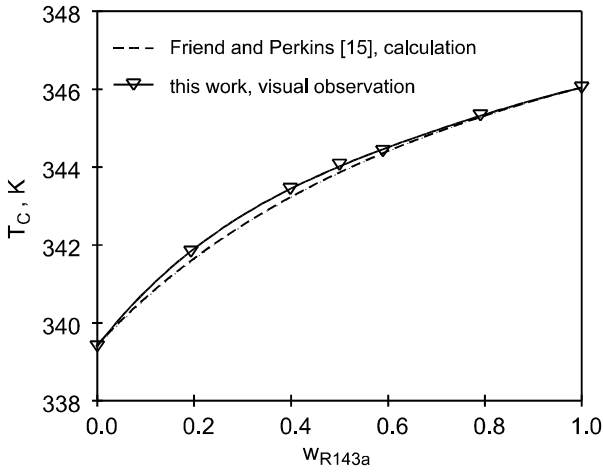

Fig. 3. Critical temperature of the binary mixture R-125/143a and its dependence on the mass fraction of R143a.

as would be expected for hydrocarbon mixtures as suggested in Ref. 18. In Fig. 3 the solid curve represents for all the critical temperatures listed in Table III a polynomial fit of the form,

$$T_C(w_{R143a}) = w_{\mathrm{R143a}} T_{\mathrm{C,R143a}} + (1 - w_{\mathrm{R143a}}) T_{\mathrm{C,R125}} + (A + B w_{\mathrm{R143a}} + C w_{\mathrm{R143a}}^2) w_{\mathrm{R143a}} (1 - w_{\mathrm{R143a}}), \quad (7)$$

where $T_{\mathrm{C,R143a}}$ and $T_{\mathrm{C,R125}}$ are the critical temperatures of the pure components R143a and R125, respectively. The values of the coefficients A, B, and C determined by a fit are 9.352 K, −11.062 and 5.449 K, respectively. Within an experimental uncertainty of ±0.05 K the composition

Table III. Experimental Values of the Critical Temperature and Their Dependence on Composition for the Binary Mixture of R143a and R125

w_{R143a}	T_{C} (K)
0.0000	339.40 [16]
0.1935	341.83
0.3988	343.44
0.5000	344.06 [3]
0.5900	344.41
0.7913	345.33
1.0000	346.04 [17]

dependence of the critical temperature of the binary mixture of R125 and R143a may well be represented by the polynomial fit according to Eq. (7). Finally, an equation for approximation of the composition dependence of the mixture critical temperature as proposed by Friend and Perkins [15] is given by the dashed curve in Fig. 3, which has been obtained from

$$T_C(x_{R143a}) = T_{C,R125} + \frac{x_{R143a} M_{R125}}{(1 - x_{R143a}) M_{R143a} + x_{R143a} M_{R125}} \times (T_{C,R143a} - T_{C,R125}), \quad (8)$$

where x_{R143a} is the mole fraction of R143a and M_{R143a} and M_{R125} are the molar masses of R143a and R125, respectively. The differences between the fit to our experimental data according to Eq. (7) and the calculation of the mixture critical temperature as given by Eq. (8) by Friend and Perkins [15] are smaller than 0.3 K.

4.4. Data Comparison

With a knowledge of the dependence of the mixture critical temperature on composition, a prediction for the desired thermophysical properties with the help of Eq. (1) is now possible for any composition. In Fig. 4 the thermal diffusivity and the sound speed of binary mixtures of R125 and R143a under saturation conditions are plotted as a function of the mass fraction of R143a at two different temperatures. The solid and dashed curves represent the simple prediction method according to Eq. (1) for the saturated liquid and vapor phases, respectively. In applying Eq. (1) the pure component data for R125 and R143a have been taken from earlier measurements [11–13], and Eq. (7) has been used to calculate the dependence of the critical temperature on the mass fraction of R143a. The symbols represent our experimental data from DLS which have been obtained from our fits from Fig 1. As can be seen from Fig. 4, the simple prediction method according to Eq. (1) reproduces the distinct behavior of both properties and their dependence on the composition very well. Similar to the dependence of the critical temperature of the mixture on its composition, as shown in Fig. 3, the mixture thermal diffusivity and sound speed show a characteristic deviation from a linear interpolation between the pure component data. This behavior is much more pronounced at higher temperatures when approaching the vapor-liquid critical point. Here, it seems that the deviations of the critical temperature from ideal mixture behavior is reflected by the curvature of the mixture data.

For the thermal diffusivity besides the deviations of the experimental mixture data from the fits according to Eq. (6), the respective deviations

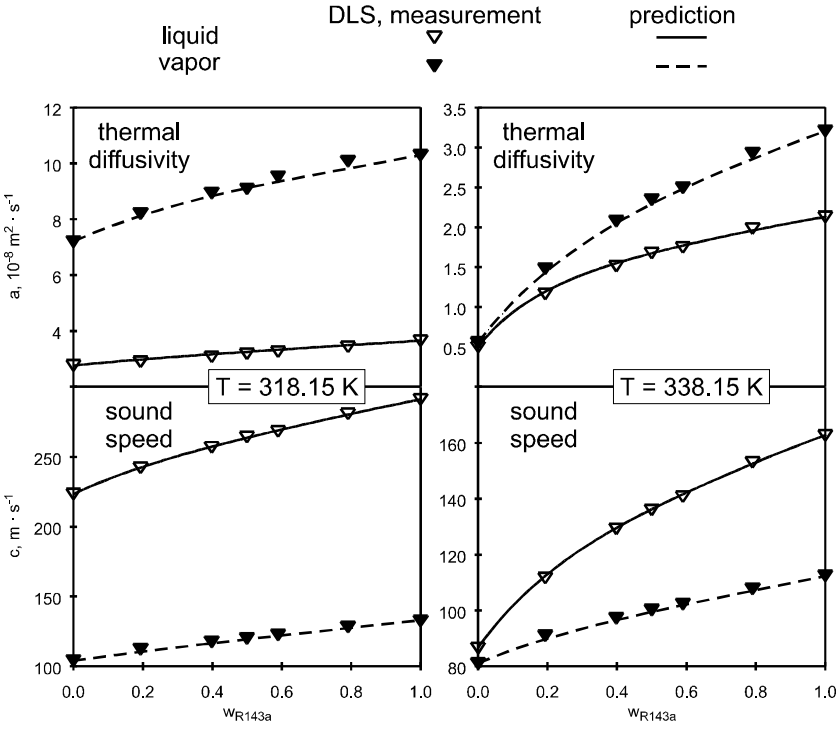

Fig. 4. Thermal diffusivity and sound speed of the binary mixture R-125/143a under saturation conditions and their dependence on the mass fraction of R143a at temperatures of 318.15 and 338.15 K.

of the proposed prediction method of Eq. (1) are also shown in Fig. 5 for the whole temperature range investigated in this work. Again, the solid and dashed curves distinguish between the predictions for the liquid and vapor phases, respectively. As can be seen from the deviation plots, for all compositions the prediction is very good with deviations typically smaller than 2–3.5 %. Only close to the vapor–liquid critical point the maximum deviations increase to 6.5 %. By that value a fundamental disadvantage of the simple prediction method is not indicated. In contrast to other prediction schemes the proposed one according to Eq. (1) allows calculation of thermophysical properties up to the critical point even though the critical temperature of one of the pure components is exceeded.

In Fig. 5 mixture data from the NIST reference database [19] and the work of Hoffmann et al. [20] are also included. For these only partial agreement can be found with our data within the combined uncertainties.

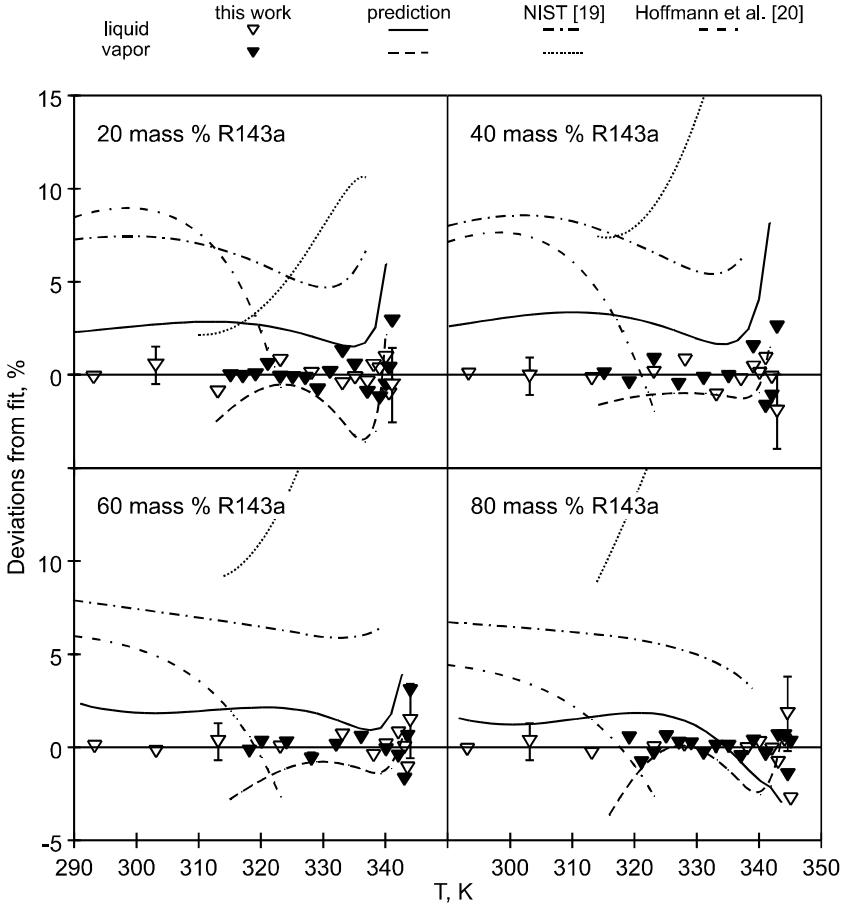

Fig. 5. Data comparisons for the thermal diffusivity of the liquid and vapor phases under saturation conditions for the binary mixture R-125/143a.

Hoffmann et al. [20] have proposed a mixing rule of Wassiljewa [21] to predict the thermal conductivity of binary systems of R125 and R143a in the saturated liquid phase on the basis of their own data for the pure components obtained by the transient hot wire technique. The prediction method of Wassiljewa [21] has been validated by Hoffmann et al. [20] through experimental investigations of the refrigerant mixture R507. However, Hoffmann et al. [20] have found deviations up to 3.5 % between their experimental data and the predicted values. Here, the thermal conductivity data predicted by Hoffmann et al. [20] have been converted to thermal diffusivity ($a = \lambda \rho^{-1} c_P^{-1}$) by using reference values for the specific heat

at constant pressure c_p of Günther and Steimle [22] and for the density ρ from the NIST database [19]. For the two mixtures rich in R143a, the differences between our measurements and the converted data of Hoffmann et al. [20] are within the combined uncertainties of the methods, if one takes into account the uncertainty of the heat capacity data of less than 1.5 % for temperatures up to 313 K and less than 2 % for the temperature range between 313 and 323 K, according to Ref. 22. In contrast, for the mixtures rich in R125, the converted data of Hoffmann et al. [20] deviate from our correlations up to +7.7 % and +8.9 %, respectively, which slightly exceeds the combined estimated uncertainties. This behavior may suggest that the mixing rule of Wassiljewa [21] can not predict the thermal conductivity of the binary mixture of R125 and R143a over a wide range of composition with sufficient accuracy.

Data compared in Fig. 5 for the thermal diffusivity from the NIST reference database [19] are based on the extended corresponding states model (ESC) for the thermal conductivity of refrigerant mixtures as proposed by McLinden and Klein [23]. The derivations of the thermal diffusivity in the NIST database [19] are carried out by converting the thermal conductivity using $a = \lambda \rho^{-1} c_P^{-1}$. Here, the thermodynamic properties of mixtures are calculated with a new model which applies mixing rules to the Helmholtz energy [24]. For the thermal diffusivity in the saturated liquid phase, maximum deviations between 7.5 % and 8.9 % can be found between the fits of our data and the values from the NIST database [19]. For the saturated vapor phase an increasing systematic positive deviation from our experimental data can be found for the values calculated by the NIST database [19] when approaching the critical point. Furthermore, with an increasing fraction of R143a the deviations are more pronounced and are up to about +35 % for the binary mixture with 80 mass % R143a. The most likely reason for this discrepancy may be found in data situation for refrigerant R143a in its gaseous state. In the NIST reference database [19] the ECS parameters for the thermal conductivity of R143a were obtained by a fitting procedure based on the experimental data of Tanaka et al. [25] for which an average absolute deviation of 14 % is stated [23].

In Fig. 6 the experimental results for the sound speed of all refrigerant mixtures investigated in this work are compared with the simple prediction method according to Eq. (1). As can be seen from the deviation plots the predictions show excellent agreement with the measured values which can be reproduced by Eq. (1) with root-mean-square deviations typically smaller than 1 %. For the saturated liquid the simple prediction method represents the measured mixture data within their experimental uncertainty except for a few values close to the critical temperature. For

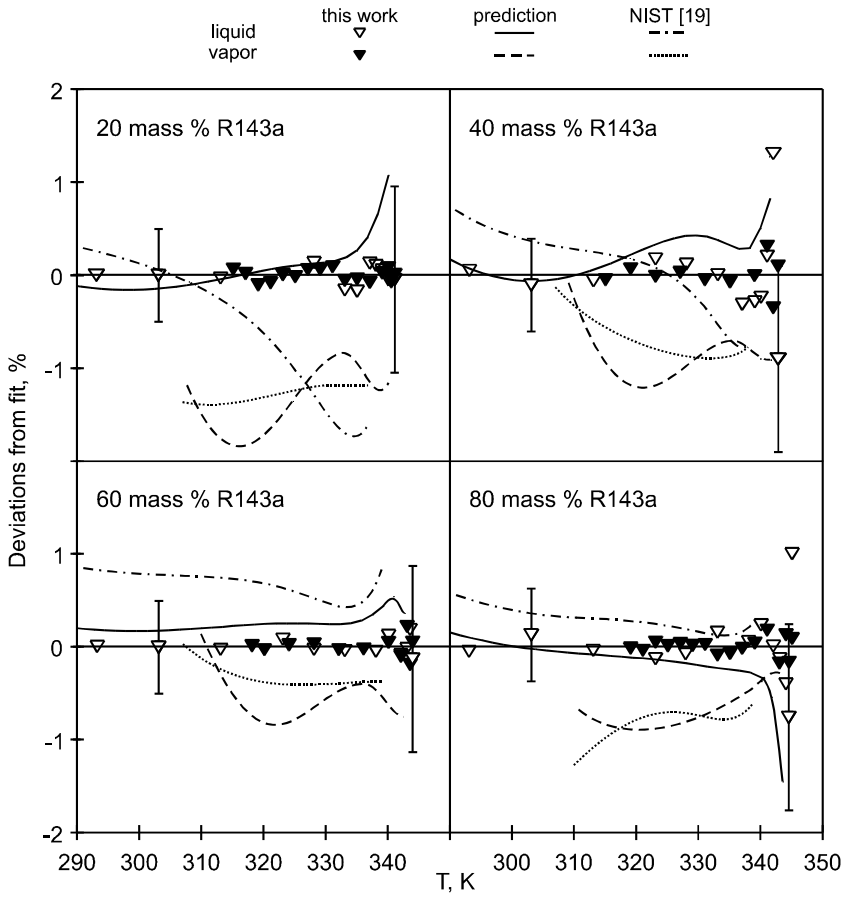

Fig. 6. Data comparisons for the sound speed of the liquid and vapor phases under saturation conditions for the binary mixture R-125/143a.

the sound speed in the saturated vapor phase it can be seen that the deviations between the experimental data and the predicted values increase slightly with an increasing concentration of R125. In Fig. 6, also included are mixture data from the NIST reference database [19] for both the liquid and vapor phases. Here, also excellent agreement with our experimental data from dynamic light scattering can be found. Data from the NIST database [19] for the sound speed in the saturated liquid phase deviate from our data set by less than 1 % except for the mixture with 80 mass % R125 when approaching the vapor liquid critical point, where the deviation increases to about 1.7 %.

5. CONCLUSIONS

In the present study the DLS technique has been applied successfully to the investigation of the thermal diffusivity and sound speed of refrigerant mixtures of R125 and R143a with a wide range of composition. The measurements cover a wide temperature range along the saturation line approaching the vapor–liquid critical point. The experimental results were used for the validation of a prediction method which can be used in a straightforward way to obtain accurate information on different thermophyical properties of multicomponent mixtures over a wide temperature range in the two-phase region up to the critical point. For all compositions the predictions show excellent agreement with the measured values. Deviations are typically smaller than 2–5 % for thermal diffusivity and 1 % for sound speed. The successful application of the prediction method is based on an exact knowledge of the critical temperature which has been determined for the mixture of R125 and R143a along with its dependence on composition in our measurements by observation of the vanishing meniscus between liquid and vapor phases. Here it seems that deviations of the critical temperature from ideal mixture behavior are reflected by the curvature of the mixture data.

In order to examine the simple prediction scheme based on the properties of the pure components as functions of the reduced temperature in more detail, further experimental and theoretical work is necessary. In future work we intend to investigate mixtures with quite disparate components to find out under what circumstances the approach fails and when it can be successfully applied.

ACKNOWLEDGMENTS

The investigated refrigerants have been provided by Solvay Fluor and Derivate GmbH, Hannover. Parts of the work were supported by the Max-Buchner-Forschungsstiftung.

REFERENCES

1. J. Millat, J. H. Dymond, and C. A. Nieto de Castro, in *Transport Properties of Fluids*, J. Millat, J. H. Dymond, and C. A. Nieto de Castro, eds. (Cambridge University Press, New York, 1996), pp. 3–5.
2. R. C. Reid, J. M. Prausnitz, and B. E. Poling, *The Properties of Gases and Liquids* (McGraw-Hill, New York, 1987).
3. A. P. Fröba, S. Will, and A. Leipertz, *Int. J. Thermophys.* **22**:1349 (2001).
4. B. J. Berne and R. Pecora, *Dynamic Light Scattering* (Robert E. Krieger, Malabar, 1990).
5. B. Chu, *Laser Light Scattering* (Academic Press, New York, 1991).

6. A. Leipertz and A. P. Fröba, in *Diffusion in Condensed Matter – Methods, Materials, Models*, P. Heitjans and J. Kärger, eds. (Springer, Berlin, 2004) pp. 571–611.
7. J. W. Schmidt and M. R. Moldover, *J. Chem. Eng. Data* **39**:39 (1994).
8. J. W. Schmidt, E. Carrillo-Nava, and M. R. Moldover, *Fluid Phase Equilib.* **122**:187 (1996).
9. A. P. Fröba, S. Will, and A. Leipertz, *Fluid Phase Equilib*. **161**:337 (1999).
10. A. P. Fröba, S. Will, and A. Leipertz, *Int. J. Thermophys.* **21**:603 (2000).
11. K. Kraft and A. Leipertz, *Int. J. Thermophys.* **15**:387 (1994).
12. K. Kraft and A. Leipertz, *Proc. Int. Conf. CFCs, The Day After* (Padova, 1994), pp. 435–442.
13. A. P. Fröba, S. Will, and A. Leipertz, *Int. J. Thermophys.* **22**:1021 (2001).
14. K. Kraft, M. M. Lopes, and A. Leipertz, *Int. J. Thermophys.* **16**:423 (1995).
15. D. G. Friend and R. A. Perkins, in *Transport Properties of Fluids*, J. Millat, J. H. Dymond, and C. A. Nieto de Castro, eds. (Cambridge University Press, New York, 1996), pp. 141–164.
16. M. O. McLinden, *Int. J. Refrig.* **13**:149 (1990).
17. L. A. Weber and D. R. Defibaugh, *J. Chem. Eng. Data* **41**:1477 (1996).
18. R. H. Perry, *Chemical Engineers' Handbook* (McGraw-Hill, New York, 1973).
19. *Standard Reference Database 14*, Version 4, Nat. Inst. Stds. Tech. (NIST), Boulder, Colorado (2000).
20. N. Hoffmann, K. Spindler, and E. Hahne, in *Bestimmung der Transportgrößen von HFKW*, Bericht zum AiF-Forschungsvorhaben Nr. 10044B, Heft 2: Wärmeleitfähigkeit, Forschungsrat Kältetechnik e.V., ed. (Frankfurt am Main, 1996).
21. A. Wassiljewa, *Phys. Z.* **5**: 737 (1904).
22. D. Günther and D. Steimle, in *Bestimmung der Transportgrößen von HFKW*, Bericht zum AiF-Forschungsvorhaben Nr. 10044B, Heft 3: Spezifische Wärmekapazität, Forschungsrat Kältetechnik e.V., ed. (Frankfurt am Main, 1996).
23. M. O. McLinden, A. Klein, and R. A. Perkins, *Int. J. Refrig.* **23**:43 (1999).
24. E. W. Lemmon and R. Tillner-Roth, *Fluid Phase Equilib*. **165**:1 (1999).
25. Y. Tanaka, M. Nakata, and T. Makita, *Int. J. Thermophys.* **12**:949 (1991).